Numerical studies of power oscillations induced by sodium boiling in ESFR after ULOF transient

X.-N. Chen *, A. Rineiski, S. Perez-Martin, E. Bubelis, M. Flad

Institute for Neutron Physics and Reactor Technology, Karlsruhe Institute of Technology, D-76344 Eggenstein-Leopoldshafen, Germany

ARTICLE INFO

Keywords:
Sodium fast reactor
Sodium boiling
Power oscillation
Unprotected loss of flow (ULOF)

ABSTRACT

This paper investigates numerically a new phenomenon of power oscillations, which is found to take place after unprotected loss of flow (ULOF) in a large power European Sodium Fast Reactor (ESFR) with a sodium plenum above the core. The oscillations are induced by sodium boiling and re-flooding events and can trigger a power excursion, if the oscillation amplitude becomes stronger and the reactivity exceeds the prompt criticality during transients. Numerical results show that after the sodium boiling onset in and in the vicinity of the sodium plenum, a negative reactivity effect is introduced, that reduces the power, and the sodium boiling is stopped. When liquid sodium re-floods into the voided region, introducing a positive reactivity effect, the power increases, and then sodium boils again. This process repeats, i.e. power oscillations take place. A long numerical simulation shows that the oscillations may disappear as the cover gas pressure increases up to a certain value during the transient. This gives us an idea that an increased cover gas pressure could prevent the oscillation for the considered case, simply because the sodium boiling is suppressed. An additional transient simulation with a higher initial cover gas pressure confirms this idea.

1. Introduction

The sodium cooled fast reactor (SFR) technology has been developed for more than 50 years. The practical experiences show its feasibility and safety potential in experimental/industrial reactors, in particular of smaller size and power. In an industrial SFR design with a power level of e.g. 3600MWth as in the European Sodium Fast Reactor (ESFR) design, the situation is more challenging, because the coolant void reactivity effect is small due to special safety design measures, but can be positive in some voiding scenario's. This is an essential safety concern for such large reactors.

The initial ESFR design was proposed by the French Atomic Energy Commission (CEA) for the CP-ESFR European Project in 2009. A high fuel volume fraction and a low sodium one were achieved in this design. A high fuel volume fraction makes utilization of fuel with a lower enrichment and elimination of fertile blankets around the core possible, while the Pu mass balance remains near zero. A lower sodium volume fraction reduces the sodium void effect in the core. Moreover, optimization studies performed for CP-ESFR have shown that a lower sodium void effect can be further achieved that would be favourable for reactor safety (Rineiski et al., 2013). However, the core cannot undergo through an unprotected loss of flow (ULOF) transient without a power excursion, since the sodium will boil and a partial core voiding gives a positive reactivity, which can lead to a prompt super-criticality during the transient, e.g. (Chen et al., 2016). The next European project on ESFR, ESFR-SMART started in 2017. For this project, a new core configuration (Rineiski et al., 2018) with a near-zero coolant void effect, mainly due to introduction of a sodium plenum above the core and core flattening, has been established. A lower axial blanket was introduced that is favourable for the void effect. An unprotected loss of flow (ULOF) benchmark was arranged and carried out in the project for the sake of reactor safety evaluation.

This benchmark shows that the ULOF transient will lead to sodium boiling and the power decreases after the boiling onset due to a negative reactivity introduction, when the sodium boiling takes place in and above the upper fuel region. However, it has been shown by calculations that the power decreasing trend may not be kept on further and the power (reactivity) oscillation could take place (Chen and Rineiski, 2022). The reason for the oscillation is, simply to say, due to the coolant re-flooding and will be discussed in detail in this paper. The oscillations according to the numerical results can be so strong, that the reactivity reaches prompt super-criticality, correspondingly resulting in a power

* Corresponding author.
E-mail address: xue-nong.chen@kit.edu (X.-N. Chen).

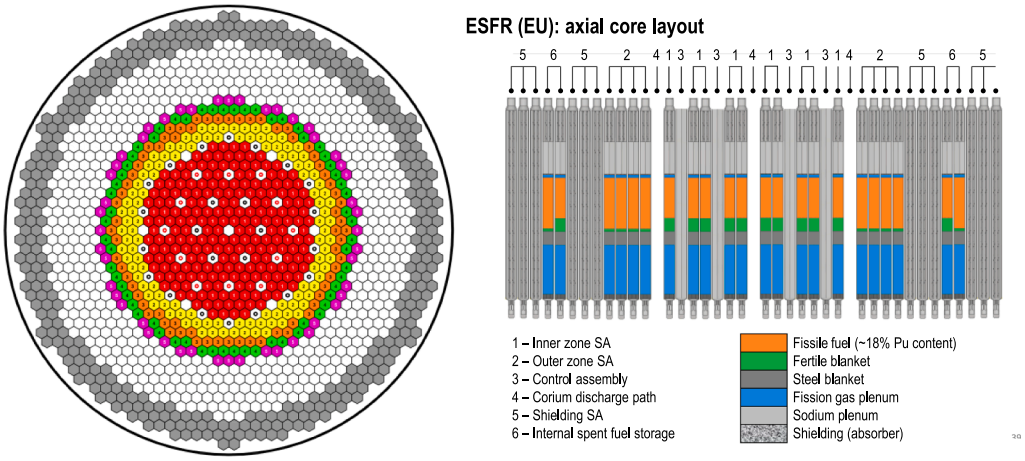

Fig. 1. Radial core map and axial core layout (Fridman and Mikityuk, 2019).

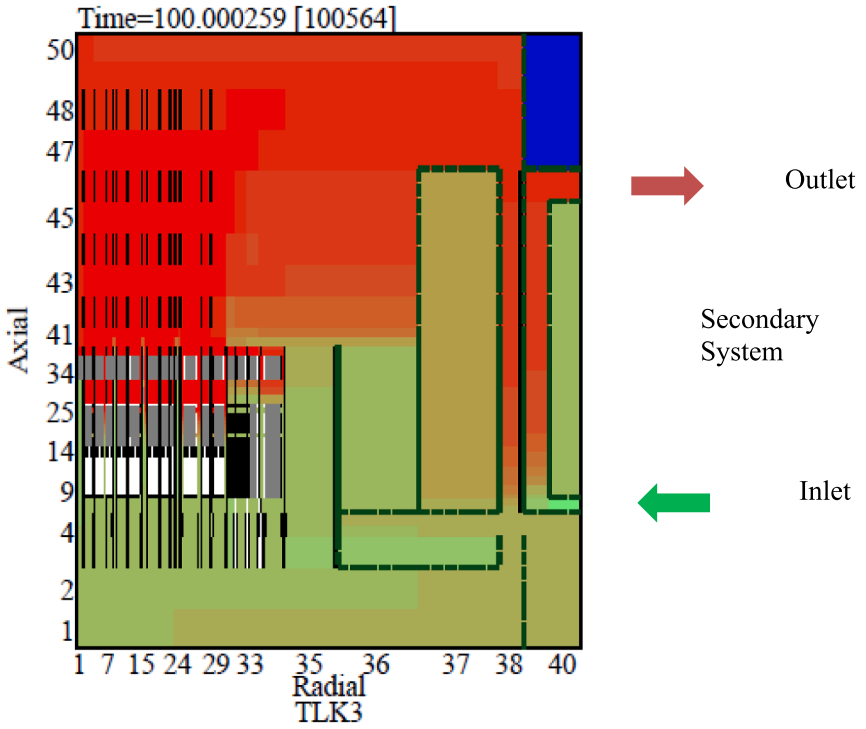

Fig. 2. SIMMER III overall simulation model with the core region from 1 to 29 in the radial direction and from 15 to 27 in the axial direction.

excursion. Therefore, it is essentially important to understand this kind of oscillations.

The power/reactivity oscillation in SFR with a sodium plenum above the core have been found recently by other researchers in their numerical simulations (Lemasson et al., 2017; Abdelhameed et al., 2021). Especially in (Lemasson et al., 2017) a ULOF transient was investigated numerically for a low void worth SFR with a nominal power of 1500MWth with two codes, namely COREMELT and SIMMER-III. As reported, the power oscillation has been found in the ULOF transient by the both codes, which is associated with sodium boiling, although the oscillation amplitude and period are quite differently predicted by them. In general, however, the phenomenon has not been fully discussed and understood, for example, what are reasons and conditions for that and if there are remedy methods for preventing a power excursion after oscillations.

The axial distribution of the coolant reactivity worth in ESFR-SMART is similar to that in a boiling water reactor (BWR), where the power oscillation or instability due to coupled thermal hydraulic and neutronic boiling effects is well-known (March-Leuba and Rey, 1993). This supports our finding basically. From the viewpoint of dynamic systems, such an oscillation belongs to a periodic limit cycle in Hopf bifurcation. It seems that the ESFR quasi-steady state during a slow transient is no longer stable and may transit to periodic oscillations, as the sodium boiling takes place.

Nevertheless, the oscillation amplitudes that were observed in the following 2D-simulations could be overestimated according to our experiences. The peak amplitude of power excursion can be smaller in case of a finer radial mesh (Chen et al., 2016) and the amplitude of power oscillations is also significantly smaller in 3D simulation (Gianfelici, 2022) than in 2D ones. This is due to artificial coincident effects in the 2D coarse radial mesh simulations. This can be a subject for future investigations.

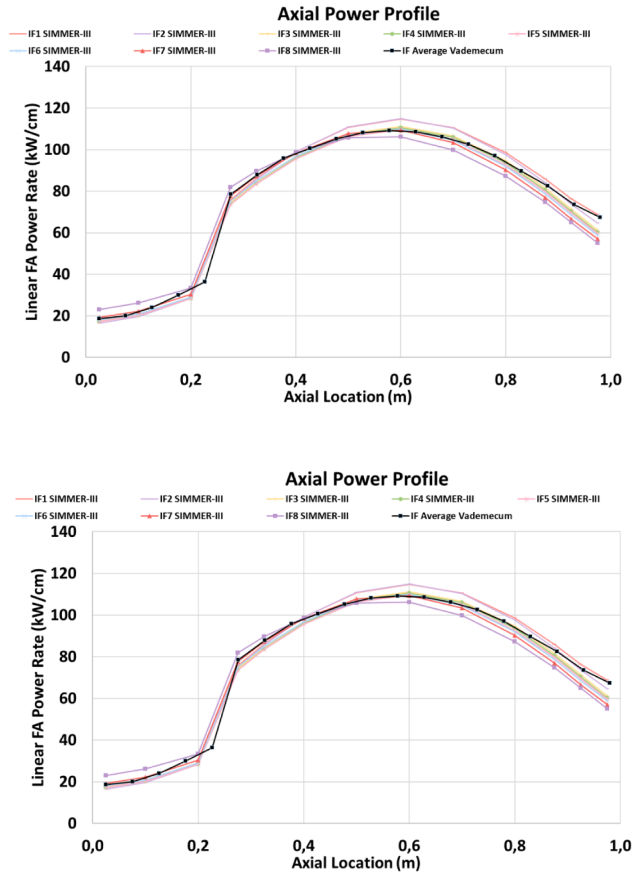

Fig. 3. Axial power profiles (linear FA power rates), the first plot for the inner core and the second one for the outer core, where the zero corresponds to the core bottom.

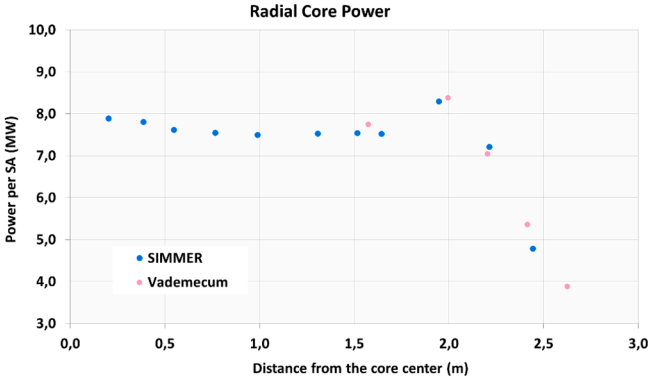

Fig. 4. Radial power profile, SIMMER vs Reference (Fridman and Mikityuk, 2019).

This paper deals with numerical simulations of the ESFR-SMART reactor with SIMMER-III code, focusing on power oscillations during ULOF transients. The steady state and ULOF calculations were carried out for benchmarks of the ESFR-SMART project. Besides the integral quantities such as power, reactivity and total mass flow rate, detailed results of mass flow rate distributions, sodium quality distribution and so on are presented for achieving a better understanding of ULOF phenomena. In order to understand the channel interaction effects, the fixed pressure boundary conditions on the core inlet and outlet have been assumed, and the results presented in the following confirm that the channel interaction does not play an essential role here. A case with an increased cover gas pressure has been also simulated, showing that it can suppress the sodium boiling and therefore suppress the sodium boiling oscillations under considered conditions.

Table 1
Neutronic parameters and feedback coefficients.

Parameter	SIMMER-III	Serpent Calculations (Fridman and Mikityuk, 2019)
K_{eff}	1.00937	1.00471
Prompt Neutron Lifetime	4.25E-07 s	4.74E-07 s
Beta Effective	347 pcm	362 pcm
Doppler Constant Fissile 1500 K => 1800 K Fertile 900 K => 900 K	808 pcm	685 pcm
Core Void Worth without Voided Gaps	1755 pcm	
Core Void Worth with Voided Gaps	1727 pcm	1542 pcm
Upper Gas Plenum + Cap Void Worth	41.3 pcm	62 pcm
Coolant Density Reactivity Coefficient	0.442 pcm/K	0.433 pcm/K
Axial Thermal Expansion Coefficient	0.0715 pcm/K	0.083 pcm/K
Radial Thermal Expansion Coefficient	0.711 pcm/K	0.646 pcm/K
Control Rod Drivelines Expansion Coefficient	423/14.5 pcm/cm	423/14.5 pcm/cm

2. SIMMER simulation model

2.1. SIMMER code

The SIMMER III/IV code (Sn Implicit Multifield Multicomponent Eulerian Recriticality), based on Advanced Fluid Dynamics Model (AFDM) (Bohl et al., 1990) and developed by JAEA (Kondo et al. 1992; Yamano, 2008), is particularly suited for studies of the secondary (transition from the degradation of the pins to full core melting and core expansion) phase of accidents such as unprotected loss of flow (ULOF). The code application range has been extended lately to simulation of the earlier transient phases, including steady state and the primary (initiating) phase. SIMMER is a Eulerian, 2D/3D multi-velocity-field, multi-phase, multi-component, fluid-dynamics code (Bohl et al., 1990; Kondo et al., 1992). It employs dedicated momentum and energy exchange models, including a fuel-pin model, to complete its macroscopic description, and coupled with a space- and energy-dependent neutron kinetics model. In this paper, 2D (R-Z) calculations are performed with SIMMER-III (release 3.F). For fluids (liquid fuel, liquid steel, liquid sodium, fuel particles, steel particles, absorber material particles and fuel chunks, gas) we use 5 velocity fields. *P*1-S4 approximation is used for neutron transport calculations and the neutron flux is discretized in 11 energy-groups.

2.2. Core configuration and SIMMER model

As already given in the ESFR-SMART document (Fridman and Mikityuk, 2019) and also reported in (Chen and Rineiski, 2022), the radial and axial core layouts are as depicted in Fig. 1. The core includes the following subassemblies (SAs): 1 central empty assembly, 216 inner core fuel assemblies (FAs) with the fissile height of 75 cm, 288 outer core fuel assemblies with the fissile height of 95 cm, 24 Control and Shutdown Devices (CSDs) and 12 Diverse Shutdown Devices (DSDs), three rows of 264 reflector assemblies and 252 spent fuel storage assemblies. The upper level of the fissile fuel is uniform, adjacent to the upper fission gas plenum, and the lower level of the fissile fuel is higher in the inner core zone, see Fig. 1. The SIMMER geometric model is set up as shown in Fig. 2 (Chen and Rineiski, 2022). The inner core is divided into 8 FA rings, the rings including 6, 12, 12, 24, 42, 54, 42 and 24 FAs in order,

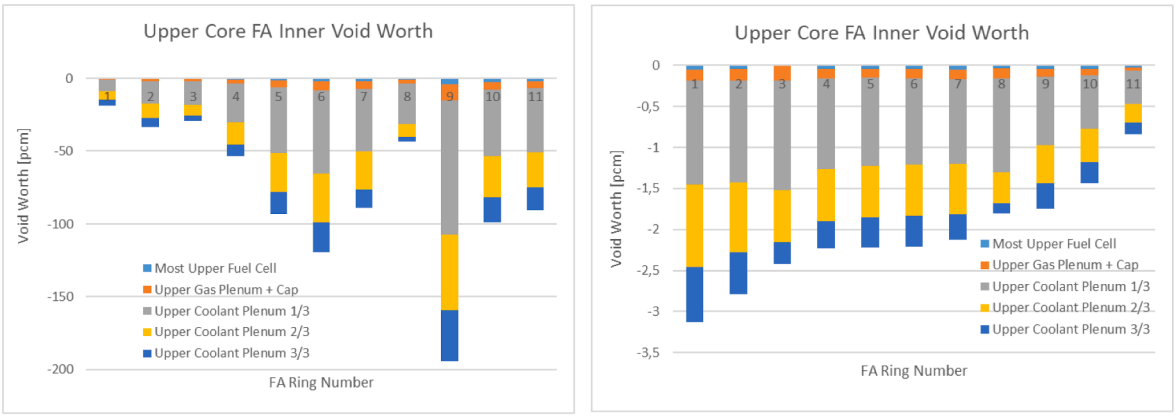

Fig. 5. SIMMER calculated sodium void reactivity worth distributions, where the worths are axially accumulated values from the uppermost fuel cell. The left plot is for whole FA rings and the right one for void worths per FA.

Table 2
Thermal hydraulic parameters for steady state.

Parameter	Design (Fridman and Mikityuk, 2019)	SIMMER-III
Total Power, MW	3600	3600
Inner Core Power per FA, MW	7.751	7.582
Outer Core Power per FA, MW	6.687	6.814
Mass Flowrate C1 per FA, kg/s	40.8	38.9
Mass Flowrate C2 per FA, kg/s	44.1	43.8
Mass Flowrate C3 per FA, kg/s	37.1	36.9
Mass Flowrate C4 per FA, kg/s (48 FA)	28.2	
Mass Flowrate C5 per FA, kg/s (60 FA)	20.4	
Mass Flowrate C4 + C5 per FA, kg/s	23.9	24.3
Coolant Core Inlet Temperature, °C	395	395
Coolant Core Outlet Temperature, °C	545	545

while the outer core 3 FA rings are with 111, 69 and 108 FAs in each FA ring. A particular aspect of this SIMMER model is that for the inter-wrapper flow spatial regions, special thin radial meshes were introduced and therefore the radial heat transfer between the SA rings have been explicitly taken into account. Moreover, the secondary circuit is included in the model in order to simulate the heat exchange with the primary-one.

2.3. *Neutronics modelling and its feedback*

The ESFR-SMART core consists of two radial parts, inner and outer cores, loaded with fuel of the same enrichment. The average Pu content in the fissile core part is about 17.9 at% at the End Of Equilibrium Cycle (EOEC), see Ref. (Fridman and Mikityuk, 2019), that includes results of neutronics calculations. In the SIMMER neutronics model the fuel composition is determined by two isotopic vectors, for "fertile" and "fissile" components, and by location-dependent values of fuel enrichment. For the ESFR-SMART, we determined initially the "fertile" vector as the average blanket isotopic composition and the fissile vector as the average core isotopic composition, so that the core enrichment is 100% and the blanket enrichment is zero in terms of these vectors. This approach, however, gives an approximate power distribution, mainly due to (1) a higher than average Pu content in the upper part of the lower blanket, and (2) a lower than average fuel burn-up at the radial core periphery. Then, the enrichments in the blanket and the last radial core ring were adjusted, i.e. slightly increased and decreased,

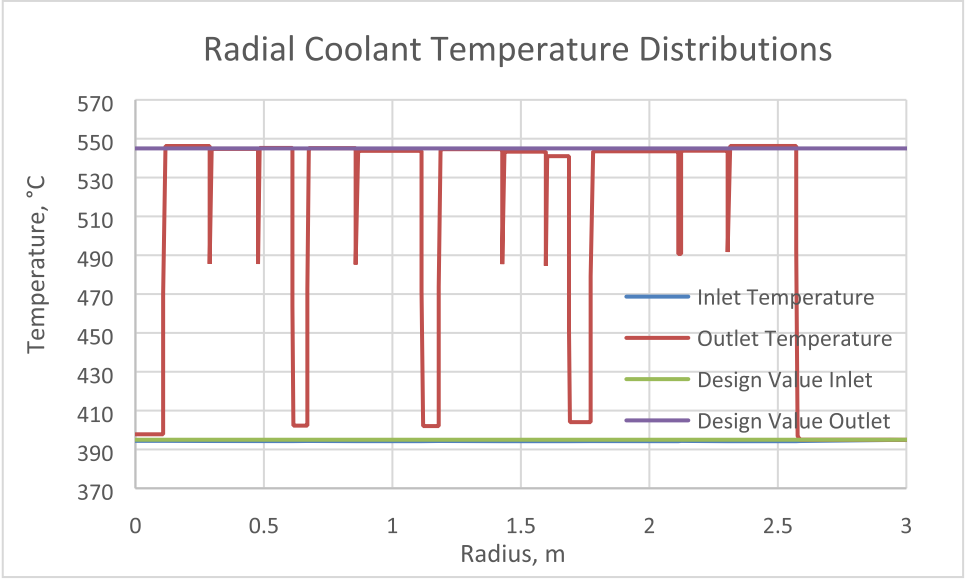

Fig. 6. Coolant core inlet and outlet temperature distributions.

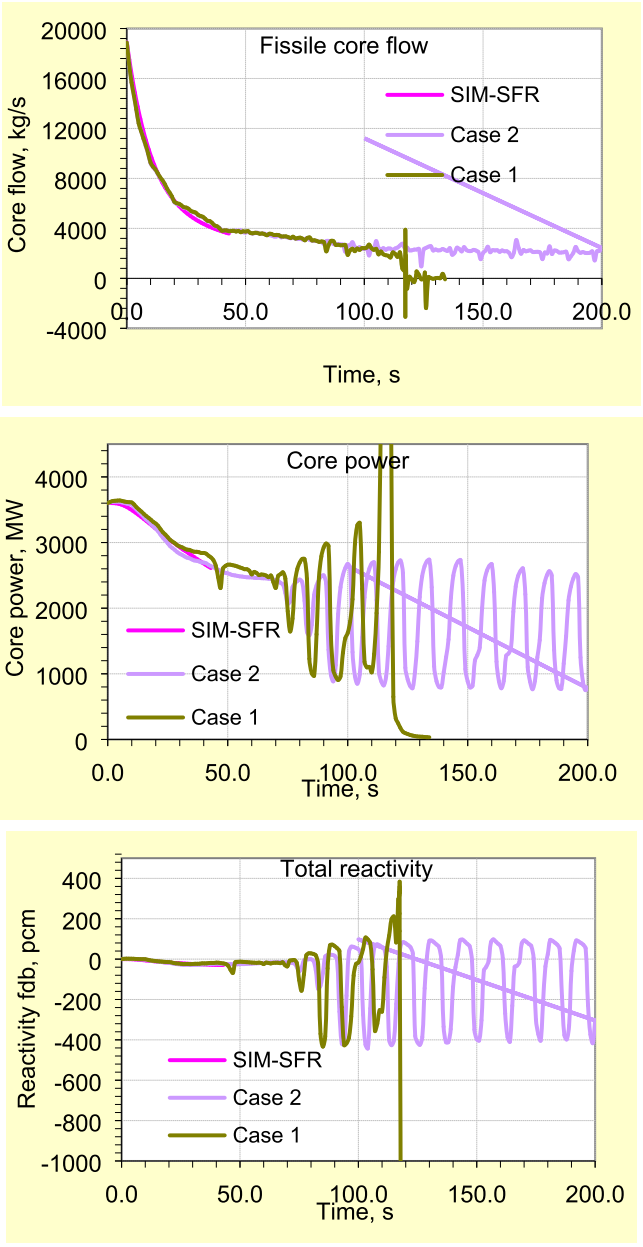

Fig. 7. ULOF Case 1 and Case 2 results of mass flow rate, power and total reactivity in comparison with SIM-SFR results.

respectively, the total fertile and fissile masses being kept. The adjustment improved SIMMER neutronics results. The results obtained with SIMMER for axial and radial power profiles are shown in Fig. 3 and Fig. 4, respectively, and they are in reasonable agreement with the project reference (Fridman and Mikityuk, 2019) results. IF/OF in Fig. 3 refer to inner/outer fissile core sub-regions with the lower axial blanket heights of 25/5 cm.

The reactivity feedback coefficients computed with SIMMER and some related values are shown in Table 1 and compared with the reference ones. The SIMMER values are in general agreement with the reference ones, the differences being related to approximations in the SIMMER neutronics model, such as the employed RZ geometry, 11 energy groups, etc. It is important to notice that the sodium void worth above the core, where sodium boiling onset takes place, is negative.

We assume that the uncertainties in the Doppler constant and sodium void effect due to nuclear data are about 10% or higher. We have not tried to reduce deviations with the reference neutronics results mainly due to this reason. Note also that the reference calculations are done in 3D for a heterogeneous geometry model with continuous-energy nuclear data, while we employ a 2D homogeneous geometry with 11-group data. On the basis of earlier studies, we expect that results will be qualitatively the same if the reactivity effects were different from the computed ones within a 10% range. A large additional effort is needed to confirm this expectation, we consider such effort for the future.

The CRDL expansion feedback was taken into account in SIMMER as in some other safety codes applied for ESFR-SMART studies. First, reactivity effects due to different CRDL insertion (CR worth curves) into the core were computed by a reference neutronics code, for single CR insertions and for insertions of groups of CR rods. In transient SIMMER calculations, we assumed the CR bottoms located at the upper fissile core boundary. The SIMMER code computed average insertion depths into the core at all times for all CRs together, while taking into account slightly temperature distributions in different radial sub-regions. These distributions were used to calculate CRDL and core thermal elongations. Due to similarities in CR insertions worths and in CRDL temperatures at different locations, we assumed this approximate procedure acceptable. It can be refined in the future by considering ring-dependent elongations CR worths, but we expect a minor effect on the results because of the mentioned similarities.

Since the coolant boiling takes place in the uppermost fuel axial region and above, the void worth distribution there is particularly important. Fig. 5 shows SIMMER calculated results, where the left plot shows the whole ring void worth and the right one the void worth per FA in the ring. The void worth is naturally stronger for a higher voided region above the core, but the worth absolute value increment vs void region height decreases with the height, tending asymptotically to zero. In the radial direction, the absolute value of the void worth per FA in the radial direction monotonously decreases with the core radius. The length of the most upper fuel cell, the upper gas plenum + cap and the upper coolant plenum is 5, 6.8, 60 cm, respectively. In Fig. 5, the void worth is an accumulated value from the uppermost fuel cell up to the upper coolant plenum.

2.4. *Thermal-hydraulic parameters and models, steady state results*

The main core thermal hydraulic parameters under steady-state conditions are listed in the following: core power 3600MWth; pump thrust 4.5 bar; core mass flow rate 18705 kg/s; bypass mass flow rate 831 kg/s; coolant inlet and outlet temperature 395 °C (668 K) and 545 °C (818 K). The core is subdivided into five cooling groups as shown in the radial core map in Fig. 1 with different colours, where the cooling group 1 is assigned to the inner core and other 4 groups to the outer core. The designed cooling groups of C1, C2, C3, C4 and C5 are assigned to SIMMER-III FA rings as following: FA1-8: C1; FA9: C2; FA10: C3; FA11: C4 + C5. The mass flow rate distribution is so gauged, that the core outlet temperature distribution is radially uniform, i.e. close in each ring to the average value. The flow gauge is realised by adding orifice coefficients at the FA inlet, which correspond to the effect of valves there.

SIMMER steady-state calculations were performed under the following conditions:

- Blasius correlation for basic friction pressure drop.
- Mass flow rate in each FA ring channel was adjusted by adding orifice coefficients at the FA inlet, so that the outlet temperature is approximately uniform at 545 °C (818 K).
- Fuel thermal conductivity: Philipponneau correlation (Philipponneau, 1992) with burn-up of 9.8% and porosity of 4.5%.
- Cover gas volume in the upper cover gas region of the reactor: 250 m^3.
- Cover gas, Xenon, is simulated with a default gas model of SIMMER
- Cover gas pressure: 1 bar.
- Pump thrust: 4.5 bar.

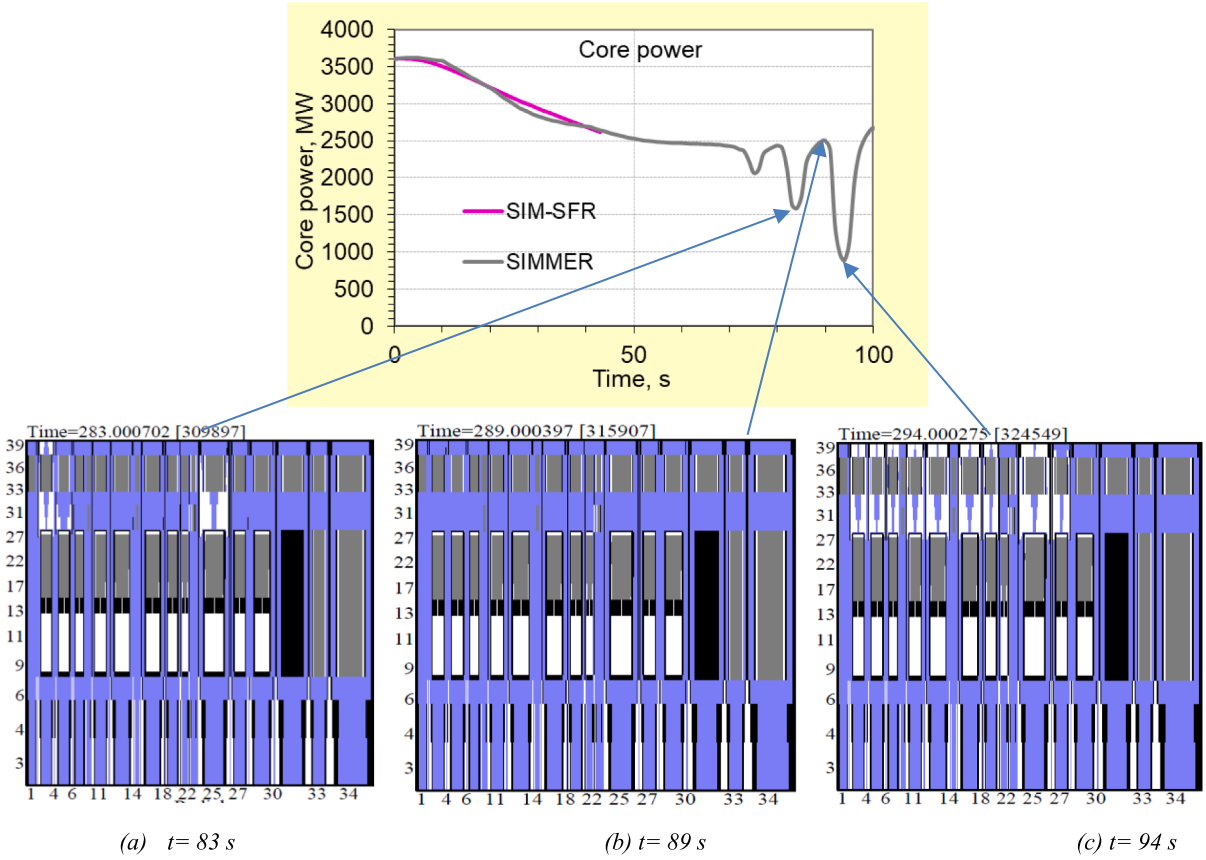

Fig. 8. Coolant void and re-flooding events, which correspond exactly to the moments of power trough and peak.

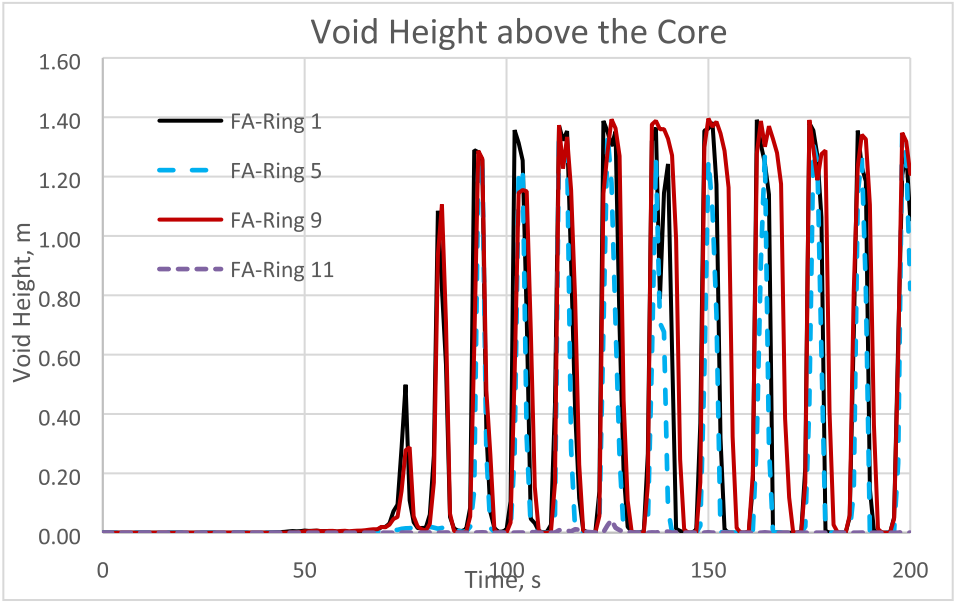

Fig. 9. Effective accumulated void height above the active region in selected FA rings.

- Fuel-clad gap conductance: simulated with a SIMMER option for variable gap conductance.

SIMMER results at steady state, including coolant mass flow rates and temperatures at EOEC conditions, have been compared and checked in the ESFR-SMART project benchmark. They are consistent with those computed by other partners. Here in this paper we only show the radial distributions of mass flow rate and power together with design values **in** Table 2. The coolant core inlet and outlet temperature distributions are given in Fig. 6, where its design values are uniform over the radius. These serve as a good basis for further ULOF transient calculations.

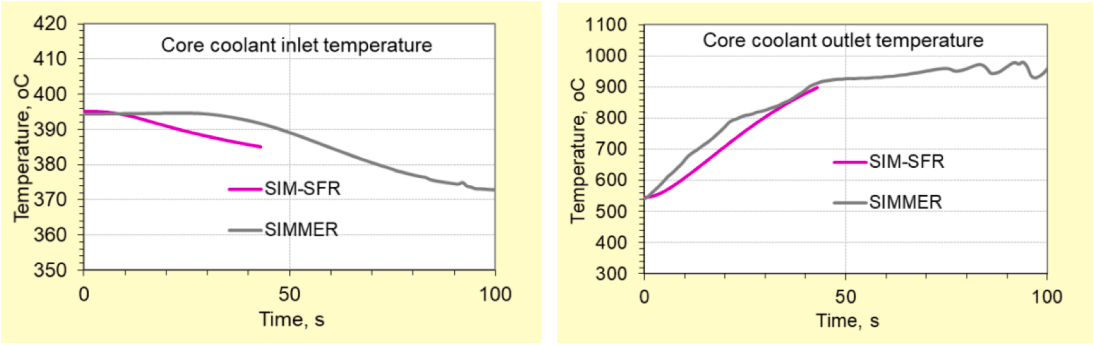

Fig. 10. ULOF benchmark of core coolant inlet and outlet temperatures.

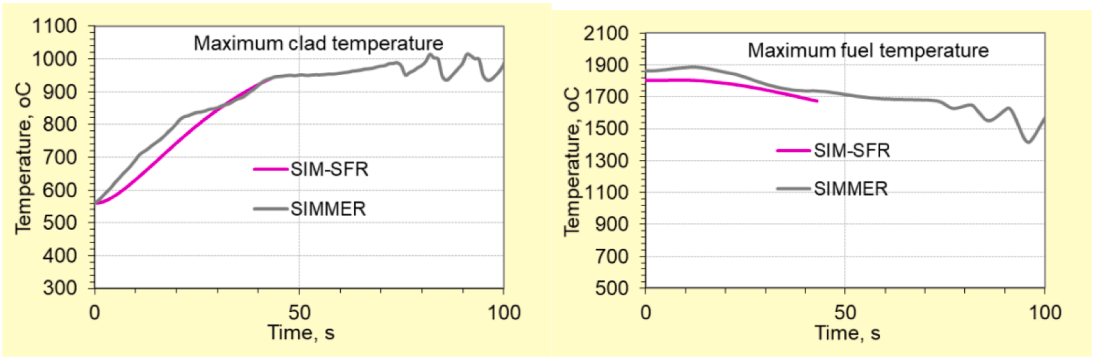

Fig. 11. ULOF benchmark of maximal clad and fuel temperatures.

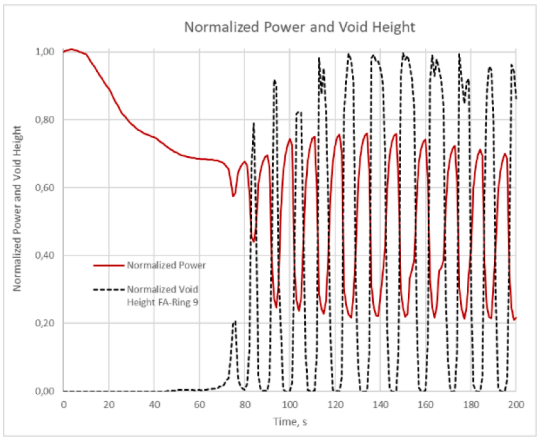

Fig. 12. The normalized power and the normalized void height in innermost FA ring of the outer core region, where the normalizing power is 3600 MW and the normalizing void height is 1.4 m.

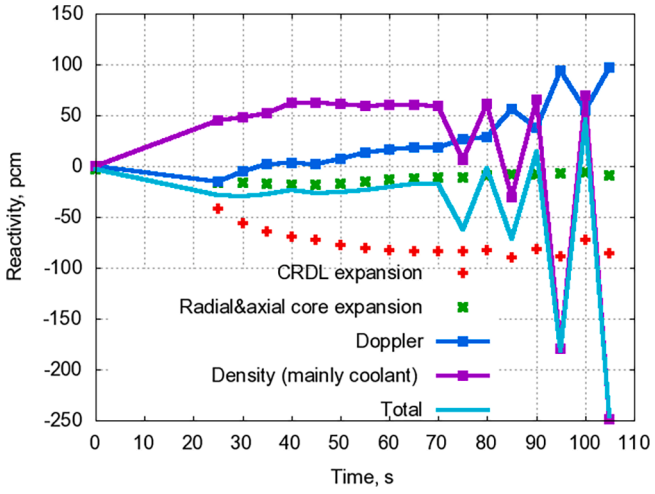

Fig. 13. Total reactivity and its components at selected time points.

3. SIMMER ULOF simulations and results

3.1. Overview of the results

Based on the steady state results, the ULOF transient has been simulated with SIMMER. The pump is coasted down with a half time of 10 s. Since the coolant inlet temperature varies slightly during the transient, the radial thermal expansion, which is assumed to be driven by the diagrid temperature so that only a small core radial size variation in the cylindrical expansion mode happens, does not introduce a significant reactivity effect. If the fuel-clad gap is closed due to irradiation, the axial core thermal expansion is driven by clad expansion, denoted in the following as Case 2; while, if the gap is open, it is driven by fuel expansion denoted as Case 1. Results for both options are given in the following. It can be understand from simulation results that the major different behaviors between Case 1 and Case 2 are that axial thermal expansion gives a positive feedback in Case 1 and a negative one in Case 2, since the fuel temperature decreases and the clad temperature increases during the ULOF transients. Simply to say, for Case 2 one gets a larger negative feedback than for Case 1 during ULOF transients. A temperature-independent thermal expansion coefficient of 1.82E-5 for the Control Rod Driveline (CRDL) has been applied, which is the reference value of the project. The times for major events as the boiling onset and the power excursion start are shown in the following as well.

Fig. 7 shows the calculated results for Case 1 and Case 2 together with SIM-SFR results, where the SIM-SFR code (Bubelis et al., 2017)

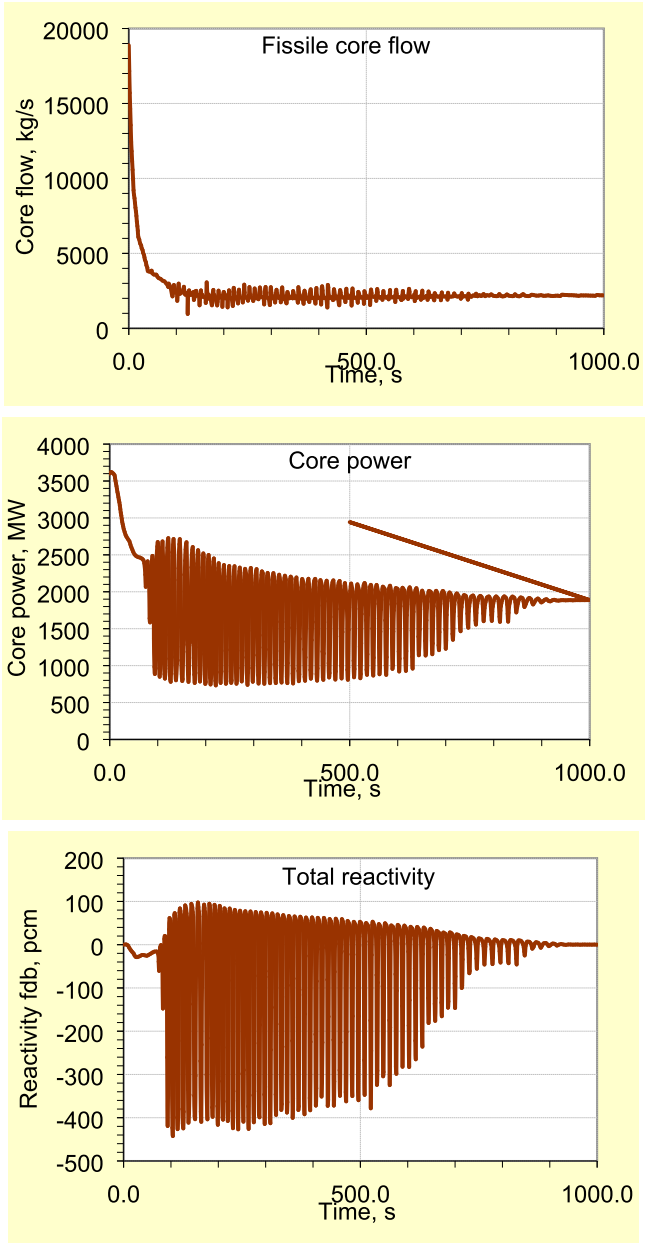

Fig. 14. ULOF Case 2 results of mass flow rate, power and total reactivity.

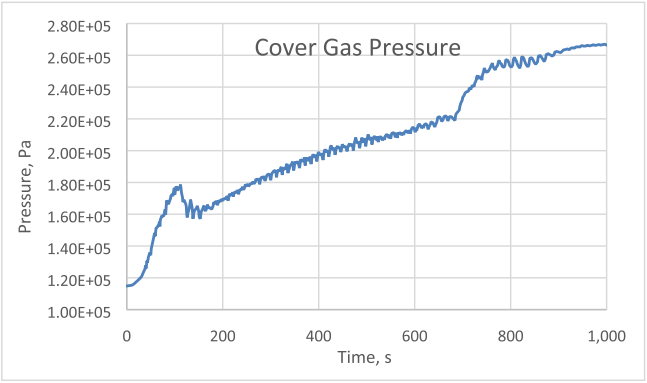

Fig. 15. Cover gas pressure history.

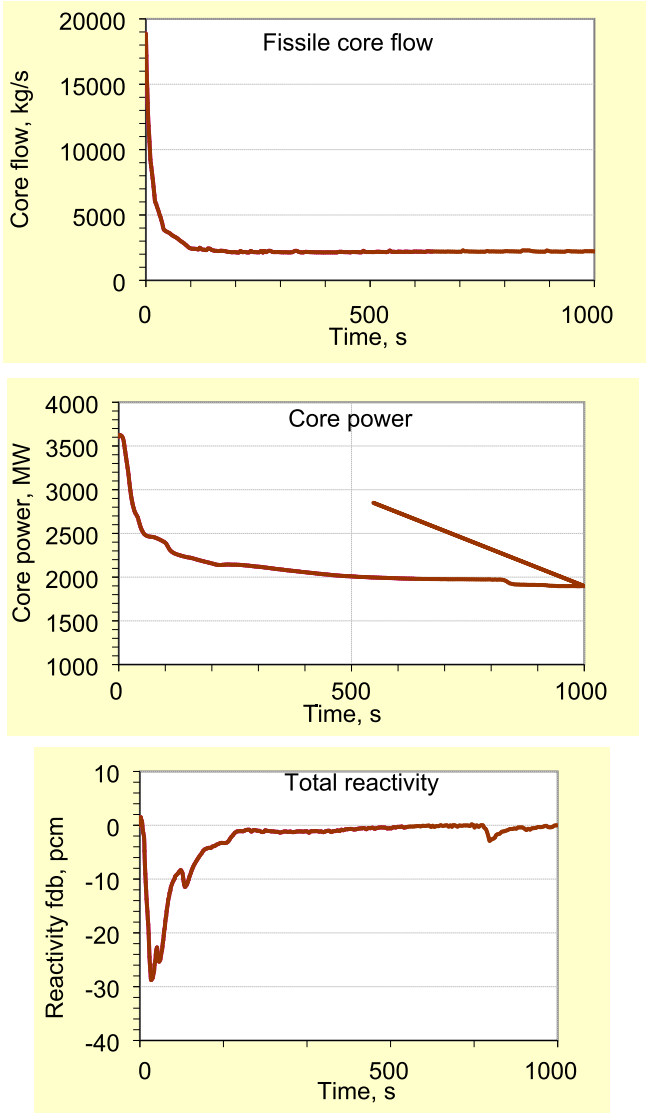

Fig. 16. ULOF results of mass flow rate, power and total reactivity, where the initial cover gas pressure is 5 bar.

employs fast-running models. The difference is due to fuel-driven and clad-driven axial thermal expansion options for Case 1 and Case 2, respectively. Case 1 results in a power excursion and core degradation, while Case 2 results only in sodium boiling, no power excursion. This is in line with earlier ESFR studies that the sodium boiling can lead to a power excursion, if the reactivity is not low enough to cope with coolant flow reduction, and the sodium boiling induces oscillation. The power excursion in Case 1 is with a peak that is about 3150 times of the nominal operational power. Case 1 will not be discussed in following sections of this paper. But Case 2 will be analysed in detail.

Both cases present oscillations in power and reactivity after the sodium boiling onset. These oscillations are discussed in detail in the following subsection.

3.2. *Analyses of sodium boiling in Case 2*

After the sodium boiling onset, one can see significant oscillations of power and reactivity, see Fig. 7. As we know, the sodium boiling takes place at the uppermost part of fuel assemblies, where the void worth is negative, as shown in Fig. 5. Thus we should understand the void distributions during the transient. Fig. 8 shows the scenarios at three typical moments of coolant voiding and reflooding, which are found to

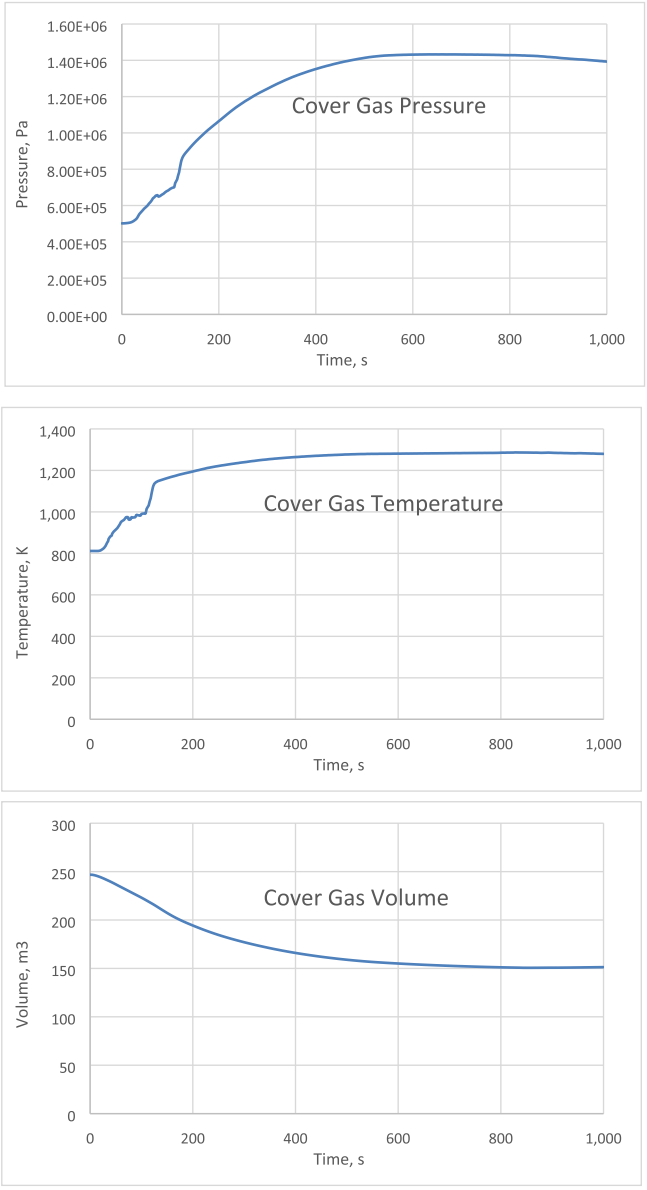

Fig. 17. Histories of cover gas pressure, temperature and volume, where the initial cover gas pressure is 5 bar.

be corresponding to the power/reactivity trough and peak values. Therefore, the sodium boiling above the core gives a negative feedback and forces the power to decrease; afterwards, as sodium comes back into the voided region due to the remained mass flow and condensation, namely a coolant reflooding, which makes the reactivity and power increase again. This procedure repeats with a period of about 10 s.

In order to give more detail of the phenomenon, we present development of the voided region heights above the core in Fig. 9. It shows that the sodium boiling takes place first at FA-ring 1 (the innermost one) and FA-ring 9 (the hottest one) and the boiling oscillation is weak and becomes stronger. After a few oscillations, the boiling propagates to other FA rings, which can be seen from the FA-ring 5 curve, as an example, in Fig. 9.

In general, the oscillation period should be associated with the heat transfer time, i.e. the time that the heat produced in the fuel pellets needs to be transferred to the sodium coolant. It includes the heat conduction time from fuel pellets to pin clads and the heat transfer time from clads to sodium bulk in the radial direction and the heat transfer through the coolant flow to the boiling region in the axial direction. Actually the instant for a maximal sodium boiling corresponds to the peak point of the heat, which is transferred and convected to the coolant in the core upper part.

Fig. 10 shows core coolant inlet and outlet temperatures. The inlet temperature is slightly decreasing and the outlet temperature is increasing as expected. The agreement with SIM-SFR and other unpublished results is again good. As the sodium boils, the outlet temperature reaches the sodium saturation point and oscillates near it afterwards.

Fig. 11 shows the maximal clad and fuel temperatures during the ULOF transient. The clad temperature increases significantly, while the fuel temperature decreases. The agreement is good again. Note that the fuel- and clad-driven axial thermal expansion effects give reactivity feedbacks of different signs: the fuel-driven one is positive, while the clad-driven one is negative. If we read the power values in Fig. 8 and the clad temperature ones in Fig. 11 on purpose, we can find that the clad temperature peaks or troughs have a 2sec delay behind the power. Fig. 12 shows the normalized power and the normalized void height in the hottest SA ring (the innermost FA ring in the outer core region), which are anti-phased. Since the sodium boiling has the same phase as the coolant absorbed thermal power, the coolant thermal power has about 180° phase shift, i.e. 5 *sec* time shift, after the fuel thermal power.

The reactivity components are evaluated at selected time points and shown in Fig. 13. This confirms again that the void reactivity (sodium boiling) is anti-phased to the power peak, as illustrated in Fig. 8 and Fig. 12.

4. Additional numerical results and discussion

There is something new in numerical results, if we consider a longer time range. Moreover, there is a directly derived method to overcome the sodium boiling problem. Therefore we address them in the following.

4.1. *Long time behaviour after sodium boiling onset in Case 2*

Case 2 can be calculated further, e.g., up to 1000 s. Fig. 14 shows the results for mass flow rate, power and total reactivity. The mass flow rate shows smallest oscillations and tends to a stable level after certain time, while the power and reactivity develop to large oscillations at first and afterwards the oscillations decay and disappear finally. If we output the pressure in the cover gas region, we will understand the reason. Fig. 15 shows the history of the pressure. It is clear that the pressure in the cover gas region increases during the transient and it reaches a high value so that the sodium boiling in the core no longer takes place. The pressure increase is due to the temperature increase there, the reduced cover gas volume due to the sodium thermal expansion in the vessel and the accumulated sodium vapour due to boiling.

4.2. *Higher initial cover gas pressure*

With the abovementioned results it is very natural to think about increasing the initial pressure in the cover gas region to prevent the sodium boiling in the transient. Therefore, we increase the pressure to 5 bar and recalculate Case 2.

Fig. 16 shows the results of recalculations for the mass flow rate, power and total reactivity, all these three quantities decrease monotonously, no sodium boiling occurs, therefore no power/reactivity oscillation takes place, and finally the system reaches a steady state. The asymptotic steady state is quite similar to the original case as shown in Fig. 14, but at the slightly higher power level of 1950 MW. Fig. 17 shows time histories of the cover gas pressure, temperature and volume. The cover gas pressure increase is due to the temperature increase and cover gas volume decrease. As checked, the three quantities obey the ideal gas equation approximately. The cover gas volume decrease is due to the coolant thermal expansion in the pool.

5. Conclusion

This paper studies the phenomenon of power oscillations induced by sodium boiling, which was found in our numerical simulation of ULOF transients in the ESFR-SMART reactor. This oscillation is a result of neutronic and thermal hydraulic coupled effects under the conditions of negative effective void worth above the core and the sodium boiling. The power trough corresponds to a void state and its peak to a re-flooding state. The key reason for the oscillation (Hopf bifurcation) is the negative effective void worth and time shift from the fission heat to the sodium boiling that takes place in the core upper part. The oscillation can become stronger and lead to a prompt super-criticality, i.e. a power excursion, while it can become weaker and go on below the prompt criticality, depending on the neutronic feedbacks and the void volume. Further numerical results show that the higher cover gas pressure can prevent the sodium boiling in the considered case, which can be considered here as a remedy method to supress the oscillation.

CRediT authorship contribution statement

X.-N. Chen: Data curation, Writing – original draft, Writing – review & editing. **A. Rineiski:** Visualization, Writing – original draft, Project administration. **S. Perez-Martin:** Data curation, Visualization. **E. Bubelis:** Data curation, Visualization, Project administration. **M. Flad:** Data curation.

Declaration of Competing Interest

The authors declare that they have no known competing financial interests or personal relationships that could have appeared to influence the work reported in this paper.

Data availability

The authors do not have permission to share data.

Acknowledgment

The research leading to these results has received funding from the EURATOM research and training programme 2014-2018 under grant agreement No 754501.

References

Abdelhameed, A.A.E., Kim, C., Kim, Y., 2021. Improved FAST device for inherent safety of oxide-fueled sodium-cooled fast reactors. Energies 14, 4610.

Bohl, W.R., Wilhelm, D., Parker, F.R., Berthier, et al., 1990. AFDM: An Advanced Fluid-Dynamics Model, Vol. I: Scope, Approach, and Summary, LA-11692-MS Vol. I. Los Alamos National Laboratory, Los Alamos, USA.

Bubelis, E., Tosello, A., Pfrang, W., Schikorr, M., et al., 2017. System codes benchmarking on a low sodium void effect SFR heterogeneous core under ULOF conditions. Nucl. Eng. Des. 320, 325–345.

Chen, X.-N., Rineiski, A., 2022. Simulations of ULOF initiation phase in ESFR-SMART with SIMMER-III. International Conference on Fast Reactors and Related Fuel Cycles FR22: Sustainable Clean Energy for the Future (CN-291), 19-22 April, Wien, Austria.

Chen, X.-N., Rineiski, A., Gabrielli, F., et al., 2016. Fuel-steel mixing and radial mesh effects in power excursion simulations. Ann. Nucl. Energy 90, 26–31.

Fridman, E., Mikityuk, K., ESFR-SMART T1.2.1 Vademecum. Technical report (2019).

Gianfelici, S., et al., 2022. Transient 3D simulations for the ASTRID reactor: preliminary results for the ULOF initiation phase. International Conference on Fast Reactors and Related Fuel Cycles FR22: Sustainable Clean Energy for the Future (CN-291), 19-22 April, 2022, Wien, Austria.

Kondo, S., Tobita, Y., Morita, K., Shirakawa, N., 2003. SIMMER-III: An advanced computer program for LMFBR severe accident analysis. Proceedings of the International Conference on Design and Safety of Advanced Nuclear Power Plant (ANP'92), Vol. IV, Tokyo, Japan, 1992, pp.40.5-1 to 40.5-11. Also JAEA, "SIMMER-III: A Computer Program for LMFR Core Disruptive Accident Analysis", JNC TN9400 2003-071.

Lemasson, D., Barjot, F., Raskach, K., Volkov, A., 2017. Benchmark between EDF and IPPE on the behavior of low sodium void reactivity effect sodium fast reactor during an unprotected loss of flow. FR17, 2017, Paper No. IAEA-CN245-177.

March-Leuba, J., Rey, J.M., 1993. Coupled thermal hydraulic-neutronic instabilities in boiling water nuclear reactors: a review of the state of the art. Nucl. Eng. Des. 145, 97–111.

Philipponneau, Y., 1992. Thermal conductivity of (U, Pu)O_{2-x} mixed oxide fuel. J. Nucl. Mater. 188, 194–197.

Rineiski, A., Vezzoni, B., Zhang, D., et al., 2013. ESFR core optimization and uncertainty studies. Proc. Int. Conf. on Fast Reactors and Related Fuel Cycles (FR13), 4-7 March 2013, Paris, France.

Rineiski, A., Meriot, C., Marchetti, M., Krepel, J., ", 2018. Core safety measures in ESFR-SMART. Proc. Int. Conf. PHYSOR 2018., 22-26 April, 2018, Cancun, Mexico.

Yamano, H., et al., 2008. Development of a three dimensional CDA analysis code: SIMMER-IV and its first application to reactor case. Nucl. Eng. Des. 238, 66–73.